Role of Fibroblast Growth Factor Receptor 2 (FGFR2) in Corneal Stromal Thinning

Roy Joseph,[1] Akosua Boateng,[1] Om P. Srivastava,[1] and Roswell R. Pfister[2]

[1]Department of Optometry and Vision Science, School of Optometry, University of Alabama at Birmingham, Birmingham, Alabama, United States
[2]The Eye Research Foundation, Birmingham, Alabama, United States

Correspondence: Om P. Srivastava, Department of Optometry and Vision Science, CBSE 215, 1025 18th Street South, Birmingham, AL 35294, USA;
srivasta@uab.edu.

Received: November 28, 2022
Accepted: August 1, 2023
Published: September 26, 2023

Citation: Joseph R, Boateng A, Srivastava OP, Pfister RR. Role of fibroblast growth factor receptor 2 (FGFR2) in corneal stromal thinning. *Invest Ophthalmol Vis Sci.* 2023;64(12):40.
https://doi.org/10.1167/iovs.64.12.40

Purpose. To determine the role of fibroblast growth factor receptor 2 (FGFR2)–mediated signaling in keratocytes during corneal development, a keratocyte-specific FGFR2-knockout (named *FGFR2cKO*) mouse model was generated, and its phenotypic characteristics were determined.

Methods. A FGFR2cKO mouse model was generated by the following method: FGFR2 flox mice were crossed with the inducible keratocyte specific-Cre mice (Kera-rtTA/tet-O-Cre). Both male and female FGFR2cKO- and control mice (1 to 3-months-old) were analyzed for changes in corneal topography and pachymetry maps using the optical coherence tomography (OCT) method. The comparative TUNEL assay and immunohistochemical analyses were performed using corneas of FGFR2cKO and control mice to determine apoptotic cells, and expression of collagen-1 and fibronectin. Transmission electron microscopic analysis was conducted to determine collagen structures and their diameters in corneas of FGFR2cKO and control mice.

Results. OCT-analyses of corneas of FGFR2cKO mice (n = 24) showed localized central thinning and an increased corneal steepness compared to control mice (n = 23). FGFR2cKO mice further showed a decreased expression in collagen-1, decreased collagen diameters, acute corneal hydrops, an increased fibronectin expression, and an increased number of TUNEL-positive cells suggesting altered collagen structures and keratocytes' apoptosis in the corneas of FGFR2cKO mice compared to control mice.

Conclusions. The FGFR2cKO mice showed several corneal phenotypes (as described above in the results) that are also exhibited by the human keratoconus corneas. The results suggested that the FGFR2cKO mouse model serves to elucidate not only the yet unknown role of FGFR2-mediated signaling in corneal physiology but also serves as a model to determine molecular mechanism of human keratoconus development.

Keywords: cornea, fibroblast growth factor receptor-2, conditional knockout mice, keratocytes, stromal thinning, corneal hydrops, keratoconus

Keratoconus (KC) is a condition of unknown causes in which the cornea assumes a semiconical shape because of noninflammatory thinning of central or paracentral corneal stroma. According to National Eye Institute reports, KC is the most common corneal dystrophy in the United States, affecting one in 2000 Americans.[1,2]

Our transcriptome (RNA sequence) analyses of human KC stromal fibroblast-derived-induced pluripotent cells (iPSC) showed the downregulation of FGFR2 expression relative to similarly derived iPSC from normal human corneal fibroblasts.[3] The FGFR2 downregulation is significant because the present literature shows that disease-specific iPSCs regain their specific disease-affected signature genes and have memory of the parental cells from which they are derived.[4] Additionally, our comparative immunohistochemical analysis also showed that stromal FGFR2 was downregulated in human KC-corneal stroma relative to the age-matched human normal corneas.[3] Presently, the potential role of FGF in KC development is elusive in spite of FGF signaling and is considered to play a pivotal role in eye development, based on its functional implication in regulation of cell differentiation, proliferation, migration, and survival in a variety of cells.[5] Interaction of FGF ligands with their signaling receptors (FGFR 1 to 4) is regulated by intracellular proteins or proteoglycan cofactors and by extracellular-binding proteins. Activated FGFRs phosphorylate specific tyrosine residues that mediate interaction with cytosolic adaptor proteins and the RAS-MAPK, PI3K-AKT, PLCγ, and STAT intracellular signaling-pathways.[6–10] The importance of FGF-signaling in the early mouse embryo is well established because the mutations in Fgf4, Fgfr2, Frs2a, Grb2, or Erk2 (Mapk1) all result in peri-implantation lethality.[11–16]

Dysregulation of FGF-signaling has been linked to several pathological conditions. It has been reported that specific deletions of FGFR aberrations were found in 7.1% of cancers, with the majority being gene amplification (66% of the aberrations), followed by mutations (26%) and rearrangements (8%).[17] FGFR2-inhibition has been targeted in multiple

cancers, and causes apoptosis, and also affects vision in patients who take FGFR2 inhibitors.[18] FGFR2-mutant mice showed progressive photoreceptor degeneration and thinning of the focal areas of the outer nuclear layer of the retina.[19] FGFR2-deletion results in significant meibomian gland (MG) acinar atrophy, and clinical manifestations of meibomian gland dysfunction in $Fgfr2^{CKO}$ mice, suggesting that MG homeostasis is FGFR2-dependent.[20] FGFR-1/FGFR2 double-knockout mice showed disrupted cerebellar size and laminar architecture resulting in impaired motor learning and coordination.[21] An increased apoptosis is seen in lens-specific FGFR2 knockout mice.[22] FGFR2-mutant mice that was generated after crossing FGFR2 flox mice with Foxg1-Cre resulted in a telencephalon-specific-Cre mouse that failed to develop eyelids and showed a thinner cornea.[23]

The above findings and our reports prompted us to generate a stromal keratocyte–specific FGFR2 knockout (FGFR2cKO) mouse model. The FGFR2cKO mice showed several phenotypic characteristics like those observed in a human KC cornea, notably progressive corneal thinning, increased corneal curvature and steepness, scarring and acute corneal hydrops, altered collagen structures, and diameters and keratocytes' apoptosis. The results suggested that the newly generated FGFR2cKO mice might serve not only as a model system to study significance of downstream targets of FGFR2-signaling in keratocytes-induced stromal development and corneal morphogenesis and homeostasis, but it would also serve as a model to elucidate the molecular mechanism of human KC development.

Material and Methods

Ethics Statement

All animal experiments were performed in accordance with protocols approved by the Institutional Animal Care and Use Committee of the University of Alabama at Birmingham (protocol no. 21422). Mice were housed in pathogen-free facilities at the University of Alabama at Birmingham. The research was performed in accordance with the ARVO Statement for the Use of Animals in Ophthalmic and Vision Research.

Generation of Conditional Knockout FGFR2KO Mouse Model on Doxycycline (Dox) Administration

Keratocan-Cre mice were obtained from Dr. Winston Kao (University of Cincinnati), and the FGFR2 flox mice were obtained from Jackson Laboratories (Jackson Laboratory, Bar Harbor, ME, USA). Transgene alleles were screened by PCR using tail DNA and following the conditions and primer pairs for keratocan Cre mice as reported earlier.[24] The FGFR2 flox mice were also screened as previously reported.[25] The following primers were used to analyze the keratocan Cre and FGFR2 flox mice:

Fgfr2 Fwd. 5′ TTCCTGTTCGACTATAGGAGCAACAGGCGG 3′
Fgfr2 Rev 5′ GAGAGCAGGGTGCAAGAGGCGACCAGTCAG3′
Keratocan F1 5′-TGG TGG CTT GCT TCA AGC TTC TTC-3′
Keratocan R1 5′-TAT CCA ACT CAC AAC GTG GCA CTG-3′

Compound transgenic mice of *keratocan rtTA-tetOCre-Fgfr2*$^{fl/fl}$ were generated via natural mating following the scheme illustrated in Figure 1. In this deletion system, Cre expression in keratocan-Cre mice can be initially induced in mice of any age by systemic administration of doxycycline (Dox), and consequently the floxed *Fgfr2* is ablated by Cre recombinase (Fig. 1). In our study, conditional knockout of FGFR2 was induced in mice by Dox chow feeding as desired. The pregnant females were fed with doxycycline food (600 mg/kg) to obtain tissue-specific knockout mice (S3888 Doxycycline 200 mg/Kg; Bioserv, Flemington, NJ, USA). FGFR2 conditional knockout mice thus obtained are referred to as FGFR2cKO mice, and the control mice used in all the experiments mentioned below are FGFR2 flox mice and keratocan Cre mice.

Immunohistochemical-Confocal Microscopic Analysis

The excised eyes from both FGFR2cKO- and control mice were fixed in 4% paraformaldehyde, and 10-µm frozen cryosections were recovered using a cryostat (Leica Cryostat, Buffalo Grove, IL, USA) at the Core Facility of Vision Sciences Research Center of University of Alabama at Birmingham (UAB). The sections were blocked in normal bovine serum (5%), followed by overnight incubation in anti-Fgfr2 rabbit polyclonal antibody (Abcam, Waltham, MA, USA) at 1:100 dilution. The sections were washed three times in PBS and incubated with a secondary goat anti-rabbit Alexa Fluor 555-labeled antibody (Invitrogen, Grand Island, NY, USA). Next, the sections were washed three times in PBS, and nuclei were stained with (4′,6-diamidino-2-phenylindole, DAPI) (Invitrogen, Grand Island, NY, USA) for 10 minutes. After a final wash with PBS, the sections were mounted on slides with Fluoromount-G (Southern Biotech, Birmingham, AL, USA). Fluorescent microscopic analysis was performed using Zeiss Axioplan 2 Imaging System Microscope (Carl Zeiss Microscopy, Thornwood, NY, USA) at the Core facility of Vision Sciences Research Center at the UAB. The confocal imaging was conducted using Zeiss LSM 710 confocal microscope (High Resolution Imaging Facility, UAB), and multiple images were taken from three FGFR2cKO mice and three control mice. Fluorescence intensity was measured using Image J analysis. Similarly, immunohistochemical analyses were conducted for the following antibodies: (A) anti-collagen 1 rabbit monoclonal antibody (Cell Signaling, Danvers, MA, USA) at 1:100 dilutions, and (B) anti-fibronectin monoclonal antibody (Thermo Fisher Scientific, Waltham, MA, USA) at 1:250 dilution. The secondary antibody used was goat anti-rabbit Alexa Flour 488-labeled antibody (Invitrogen, Grand Island, NY).

Western Blot Analysis

Western blot analysis was done using the procedure as described earlier.[26] The following antibodies and dilutions were done as per suggestion of the manufacturer: (1) anti-Fgfr2 rabbit polyclonal antibody (Abcam), (2) anti-collagen 1 rabbit monoclonal antibody (Cell Signaling), (3) anti-GAPDH rabbit monoclonal antibody (Cell Signaling), (4) Secondary antibody – highly adsorbed Goat anti rabbit 800 (Li-Cor, Lincoln, NE, USA).

TUNEL Assay

Tissue sections were fixed in 4% paraformaldehyde in PBS, pH 7.4 for 20 minutes at room temperature. The sections

Investigative Ophthalmology & Visual Science

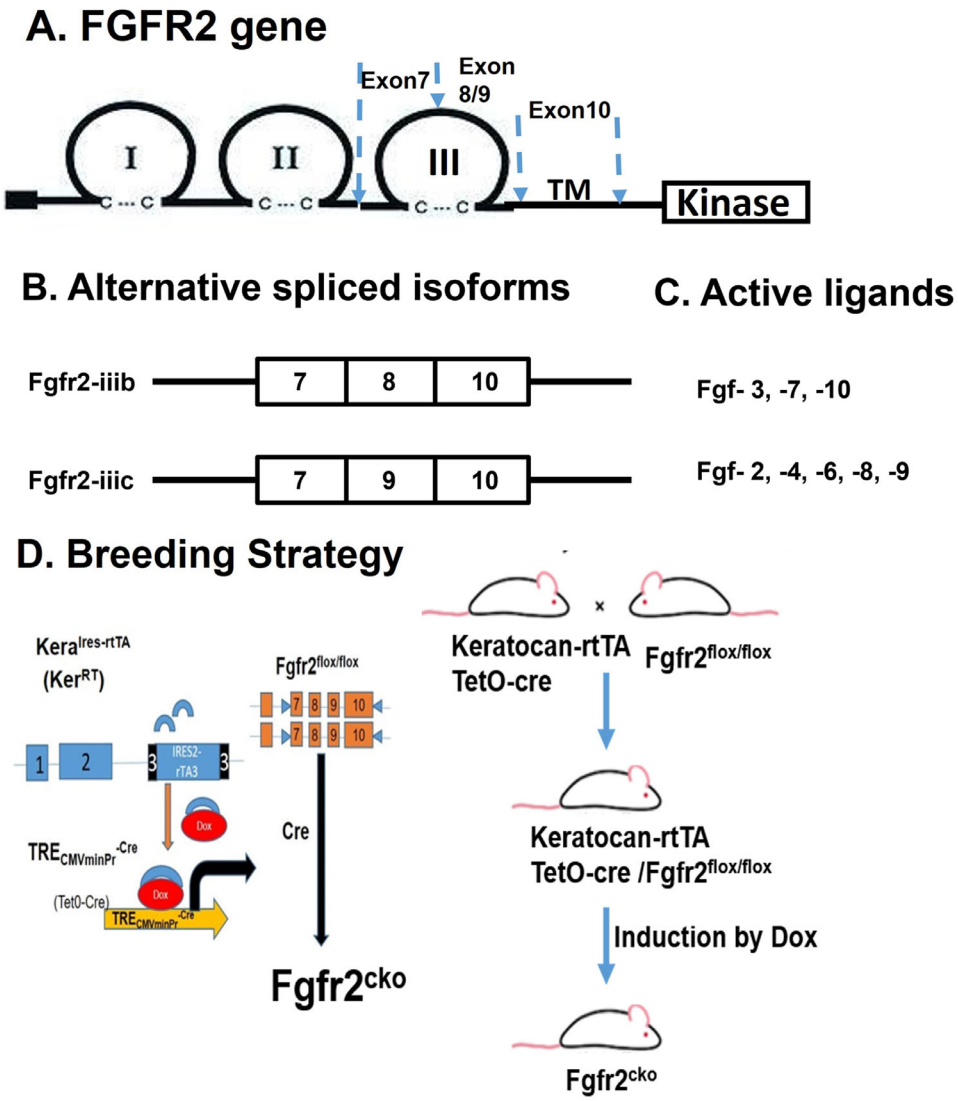

Figure 1. Generation of conditional FGFR2 knockout mice breeding strategy. (**A**) Diagrammatic representation of FGFR2 gene. (**B**) Alternative splice variant of FGFR2 gene. (**C**) Specific ligands for the Fgfr2 splice variants. (**D**) Breeding strategy. (**E**) Genotyping of FGFR2 flox mice and keratocan-Cre mice. The PCR products were analyzed using 2% agarose gel electrophoresis.

were then washed for 30 minutes in PBS, followed by incubation with 0.1% Triton X-100, 0.1% sodium citrate for two minutes on ice. Next, the sections were rinsed with PBS, and the TUNEL Reaction mixture (In Situ Cell Death Detection kit, 11684795910, Roche Diagnostics, Indianapolis, IN) was added to the sections for 60 minutes in a humidified cham-

Investigative Ophthalmology & Visual Science

ber at 37°C. The sections were washed with PBS, stained with DAPI nuclear-stain, and covered with coverslips. The fluorescence staining in cells of sections was visualized using Zeiss Axioplan 2 Imaging System Microscope (Carl Zeiss Microscopy) at the core facility of Vision Sciences Research Center at the UAB. The TUNEL-positive cells were quantified by counting them under a fluorescent microscope.

In Vivo Mouse Eye Examinations

Slit-Lamp Microscopy

Before examination, the mice were sedated using the ketamine-xylazine cocktail (0.1 mL/10 gm of body weight), with the delivered dose of ketamine, 100 mg/kg/Xylazine, 2 mg/kg. The drug was intraperitoneally injected in mice using a 1 mL syringe with a 23- to 25-gauge 5/8-inch needle. The mice pupils were dilated with eye drops containing 1% tropicamide and 5% phenylephrine hypochloride and GenTeal Lubricant Eye Gel (Alcon, Ft. Worth, TX, USA), and the mixture was applied after anesthesia until the eye examination started. Systane lubricant eye drops from Alcon were applied throughout the eye examination to avoid corneal dryness. After 15 to 20 minutes, eyes were examined using a micron IV slit-lamp (Phoenix Research labs, California) at the Vision Science Research Center Core Facility of the University of Alabama at Birmingham.

Optical Coherence Tomography (OCT)

The sedation protocol for mice was like as described above under slit-lamp analysis. Following sedation, the mouse eyes were analyzed using ANTERION OCT (Heidelberg Engineering Inc., Franklin, MA, USA) and Spectral-Domain Optical coherence tomography (SD-OCT) to visualize the anterior segments in mice as described earlier.[27,28] The anterior chamber structure and corneal curvature of the anesthetized mice were examined using Bioptigen Spectral-Domain Ophthalmic Imaging System.[29] Briefly, we used a 12 mm telecentric probe and set the reference arm at position 245. Three scans were obtained for each mouse eye, producing one rectangular and two radial scans.

Electron Microscopy Analysis of Corneas

A modified Deerinck method was used to enhance cellular components for electron microscopy analysis.[30] Eyes were fixed in Karnovsky's fixative for three hours at 4°C.[31] After the fixation, the eye samples were washed in cacodylate buffer for 10 minutes before transferring them in a solution containing 1.5% potassium ferricyanide/1% osmium tetroxide in cacodylate buffer for one hour. After washing in distilled water for 30 minutes, samples were sequentially placed for one hour in 1% aqueous thiocarbohydazide, 1% osmium tetroxide, and 1% aqueous uranyl acetate. After each staining step, the samples were washed in distilled water for 30 minutes. Next, the samples were incubated in a solution of lead aspartate in an oven at 60°C for one hour. After the lead-staining, the samples were washed two times with distilled water for 30 minutes each time. Finally, the samples were dehydrated in series ethanol solution from 70% through 100% via acetone infiltration and embedded in CY212 (TAAB) epoxy resin and polymerized for 48 hours at 60°C.

Transmission Electron Microscopy

Deerinck-Stained Samples. Ultrathin eye sections (90 nm) were cut using the Leica UC6 ultra-microtome, collected on 300 hexagonal copper grids, and analyzed using the JEOL 1010 transmission electron microscope at the High-Resolution Imaging core facility of University of Alabama at Birmingham.

Cuprolinic Blue–Stained Samples. Ultrathin (90 nm) eye sections were sectioned using Leica UC6 ultra-microtome and collected on 300 hexagonal copper grids. The copper grids were further stained with 0.5% aqueous uranyl acetate for 10 minutes. Next, the stained samples on grids were washed with distilled water and left to dry for 24 hours before their imaging using the JEOL 1010 transmission electron microscope.

Image J Analysis

The diameter of the fibers was measured at the region of corneal stromal thinning. The diameters of the individual collagen fibers were measured using Image J. The Scale bar in the figure was measured and this was used for setting the scale in the program. A line tool was used to measure the diameter of each individual fiber from both control and Fgfr2cKO mice EM microphotographs.

Statistical Analysis

The statistical significance was determined by Student's *t*-test and with statistical significance set at $P < 0.05$.

Power Analysis

Power analysis was based on the following Power 80%, 5% significance and two sided, assuming a signal/noise ratio of 1 (Cohen d, medium in the case of animal experiments). The number was a minimum of 17 mice in each group.

Results

FGFR2 Expression in Conditional FGFR2cKO Mice Compared to Control Mice

The loss of FGF-mediated signaling has been shown to inhibit normal wound healing,[5] cell survival, and dedifferentiation of myofibroblasts into fibroblasts.[32] Furthermore, our data and the present literature show that the loss of FGF-signaling occurred at the FGF2 receptor (FGFR2) level.[3] To further elucidate the role of FGFR2-signaling pathway in the corneal stromal physiology and diseases, we generated a novel FGFR2-conditional knockout (FGFR2cKO) mouse model, in which FGFR2 gene was conditionally deleted in stromal keratocyte using a keratocyte-specific keratocan-Cre mice at postnatal day 1 (P1). The FGFR2-expression in the cornea was analyzed by immunofluorescence methods in corneas of both one-month-old control- and FGFR2cKO mice (Figs. 2A–D). FGFR2- expression was observed in the corneal epithelium, stroma, and the endothelium of the normal (control) mice (Figs. 2A, 2B). A small corneal portion in Figure 2A was enlarged as shown in Figure 2B, which showed that the FGFR2-expression occurred in all the three corneal regions (Fig. 2B). As in the control mice cornea, a small corneal tissue section of FGFR2cKO mice was enlarged

Investigative Ophthalmology & Visual Science

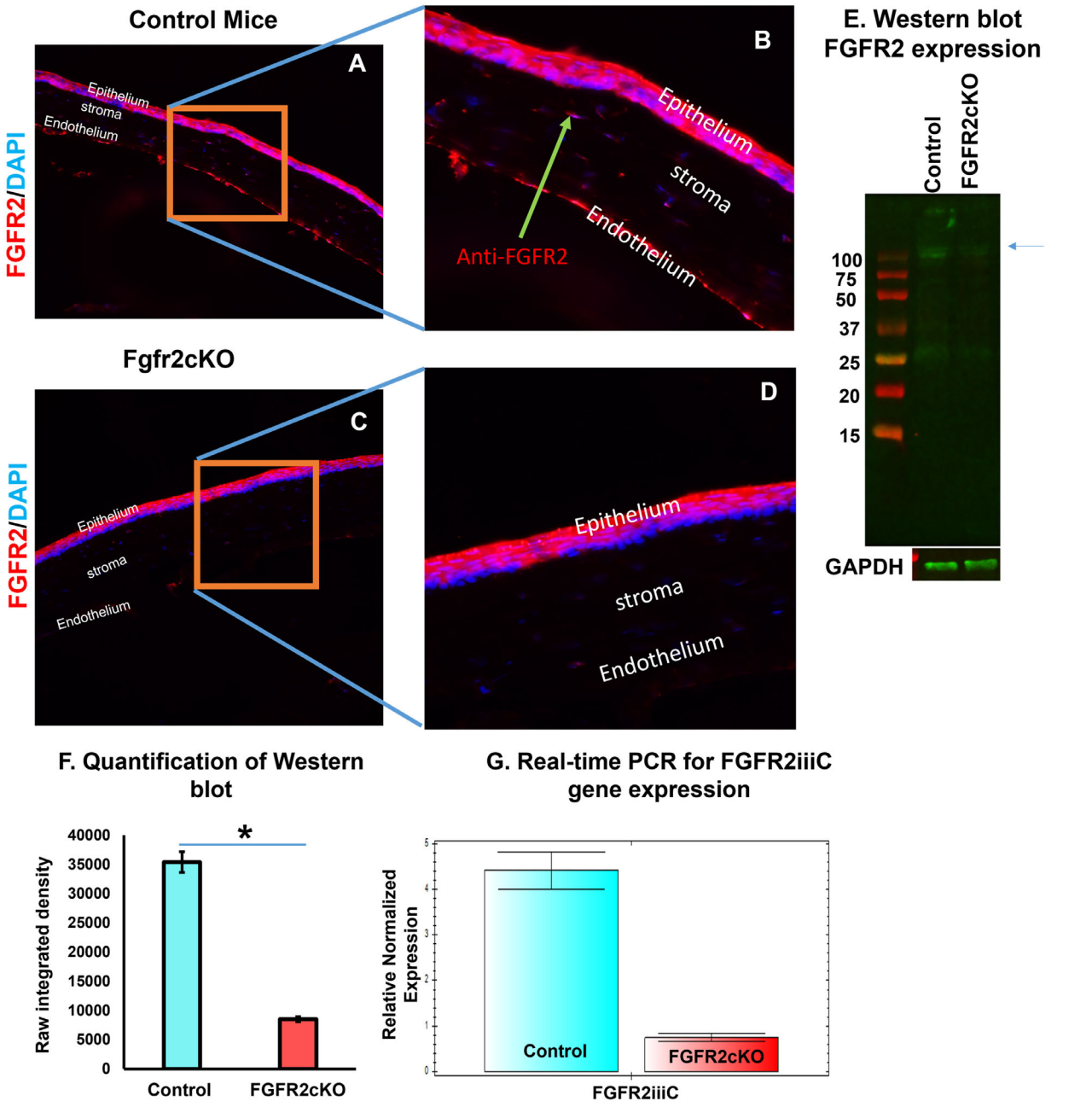

Figure 2. **(A–D)** Immunohistochemical localization of FGFR2 expression in the corneas of FGFR2cKO- vs. Control mice. **(A, B)** Immunohistochemical localization of FGFR2 expression in control mice and **B** is the magnified region of the inset as shown in **A**. **(C, D)** Immunohistochemical localization FGFR2 expression in FGFR2cKO mice, and **D** is the magnified region of the inset as shown in **C**. The results show that the FGFR2 expression is decreased in the stromal region of FGFR2cKO mice relative to control mice. (**E**) Western blot analysis of FGFR2 expression in corneal stromal of FGFR2cKO versus control mice. GAPDH was used as a loading control. (**F**) Quantification of western blot results of (**E**) using Image J. (n = 3. *$P < 0.05$). (**G**) Real-time PCR for FGFR2iiiC gene expression in the stroma of Fgfr2cKO versus control mice.

(Fig. 2D). There was decreased FGFR2 expression in the stromal region of FGFR2cKO mice relative to control mice. However, the identical levels of FGFR2-expressions in the epithelium of FGFR2cKO- and control mice were observed (Figs. 2B, 2D). However, the FGFR2 expression was relatively decreased in the endothelium of FGFR2cKO mice (Fig. 2D). The loss of FGFR2 expression in the stromal region was further confirmed by Western blot analysis of FGFR2cKO mice compared to control mice, where GAPDH was used as a loading control (Fig. 2E). The uncropped GAPDH is provided as Supplementary Figure S1. On quantification by image J of the FGFR2 band in the Western blot, the FGFR2 expression was decreased more than sixfold in FGFR2cKO mice relative to control mice (Fig. 2F, $n = 3$ [$P < 0.05$]). We further analyzed whether the stromal-specific splice variant of FGFR2 (FGFR2iiiC) was present in the stroma. This was confirmed by real-time PCR analysis of FGFR2iiic transcripts, which showed a decreased level in

Investigative Ophthalmology & Visual Science

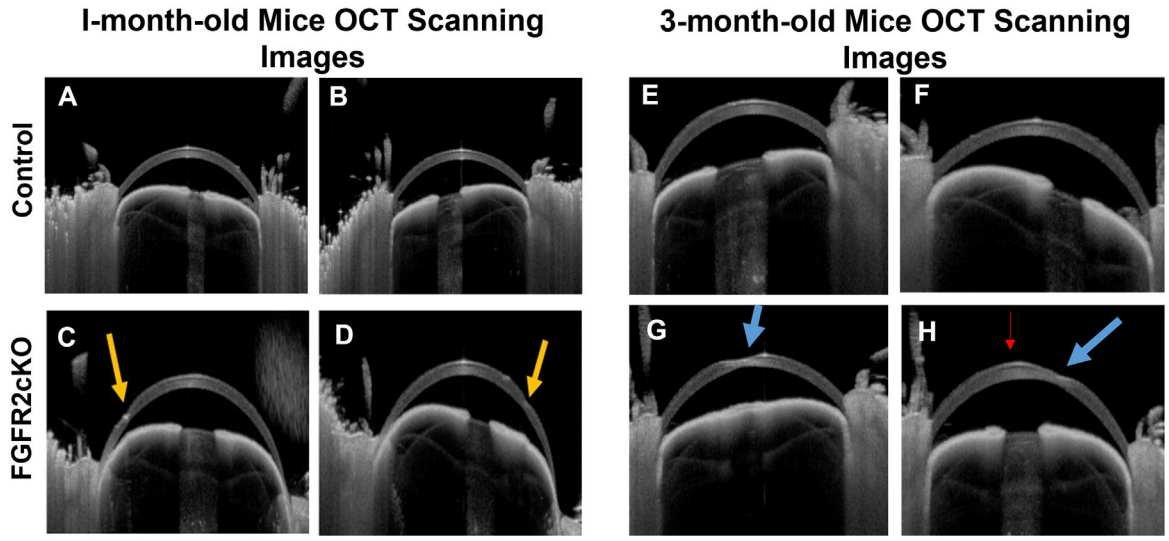

Figure 3. **(A–H)** Representative ANTERION OCT-scanning photographs of control (**A, B, E, F**) and FGFR2cKO mice (**C, D, G, H**). Scanning of control mice (**A, B**) and FGFR2cKO mice (**C, D**) was done at post-natal (*P*) 31 days. The *yellow arrow* on **C** and **D** points to the region of corneal thinning and scarring in the FGFR2cKO mice at P31 compared to the control mice (**A, B**), which lacked corneal thinning and scarring. The same FGFR2cKO- and control mice (scanned at P31 [**A–D**]) were later scanned at P90 (**E–H**). Scanning photographs of FGFR2cKO mice (**G, H**) at P90 days exhibited thinning and scarring (*blue arrows*) with no such thinning and scarring in control mice (**E, F**). The *red arrow* points to corneal cone formation in the FGFR2cKO mice. In FGFR2cKO mice, the localized thinning that was seen at P31 **(C, D)** further progressed to the central region **(G, H)** at P90 days compared to control mice which showed no thinning.

the stroma of FGFR2cKO mice compared to the control mice (Fig. 2G).

Corneal Stromal Thinning in FGFR2cKO Mice Relative to Wild Type Mice

We used a variety of techniques which included SD-OCT scanning, ANTERION OCT, histological staining, and slit-lamp bio-microscopy to visualize the anterior segment of the eye including the cornea. Figures 3A and 3B show the representative scanning images on ANTERION OCT analyses of eyes of two 1-month-old FGFR2cKO- and WT mice (n = 6 of both types). Figures 3C and 3D show similar analyses of eyes of two 1-month old-FGFR2cKO mice. The corneas of FGFR2cKO mice showed localized thinning at the peripheral region (shown by yellow arrows in Figs. 3C and 3D relative to WT mice in Figs. 3A and 3B). When the eyes of the same one-month-old FGFR2cKO- and WT mice were scanned at three months, FGFR2cKO mice developed more central corneal thinning (shown by blue arrows in Figs. 3G, 3H) relative to WT mice (Figs. 3E, 3F). FGFR2cKO mice also showed deep anterior chamber (Fig. 3H) relative to WT mice. The observed progressive corneal central thinning seen at three months as opposed to peripheral thinning at one month in FGFR2cKO mice is a significant observation because three months of mice age corresponds to the teenage human years and represent the time when human KC is manifested.

We had to switch to SD-OCT analysis method because ANTERION OCT files could not be used for topographic mapping. Figure 4A bar graph shows the number of animals used for SD-OCT scanning. Both keratocan-Cre and FGFR2-flox mice were used as controls. When 23 control mice (three months old) were scanned, two mice of the control group exhibited abnormalities in their corneas. Similarly, when 24 FGFR2cKO mice (three month old) were scanned, among these 20 mice showed corneal thinning, and only four FGFR2cKO mice had a normal cornea (Fig. 4A). The Table summarizes the clinical findings of the 24 FGFR2cKO mice. The representative SD-OCT images (Figs. 4B–D) are of 3 control mice corneas whereas Figures 4E to 4G are of three FGFR2cKO mice corneas. Figure 4G also shows a characteristic cone formation in the FGFR2cKO mice, which was not seen in the control mice. In summary, the corneas of FGFR2cKO mice showed characteristic phenotypes of localized thinning and an increased anterior chamber depth.

Topographical and Pachymetry Maps Generated for FGFR2cKO- and WT Mice Using OCT Data

Because there is no instrument available to analyze the topographical and pachymetric maps of small animals such as the mouse cornea, we used calibrated mouse corneal OCT scans and generated mouse anterior axial maps (corneal curvature) and pachymetric maps (corneal thickness) of control- and FGFR2cKO mice.[33] Figures 5A and 5B are representative images of the axial- and pachymetric maps of the corneas of control mice, respectively. Similarly, Figures 5C and 5D are representative images of corneal axial and pachymetric maps of FGFR2cKO mice, respectively. Relative to control mice, the FGFR2cKO mice exhibited an increased corneal steepness as shown in the axial map, considerable thinning of the cornea, and an irregular astigmatism.

Collagen-1 Expression in Corneas of FGFR2cKO and Control Mice

It has reported that structural deformity in the cornea may be dependent on the expression of collagen fibrils.[34] Since our mice showed changes in their corneas when observed using

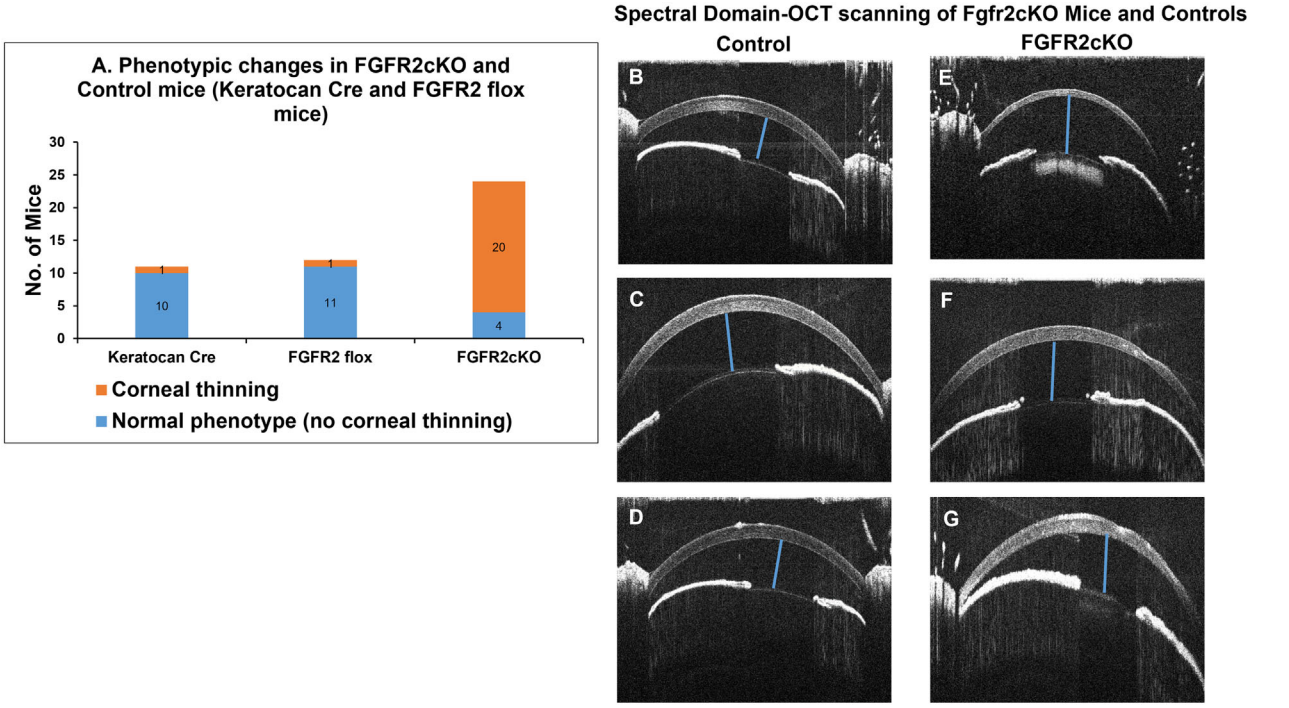

Figure 4. Spectral domain OCT scanning of FGFR2cKO mice and controls. **(A)** Phenotypic changes observed in number of mice during OCT scans in control mice (Keratocan-Cre and FGFR2 flox mice) and FGFR2cKO mice. The mice numbers in *blue color bars* show the normal phenotypes (no corneal thinning) in control mice (Keratocan-Cre, FGFR2flox) and FGFR2cKO mice, whereas the orange bars show the relative number mice of the three types of mice that exhibited corneal thinning. **(B–D)** Representative spectral domain OCT of control mice and **(E–G)** representative spectral domain OCT of FGFR2cKO mice.

Table. Summarizing the Clinical Findings of Fgfr2cKO Mice

No.	Mouse Identifier (Cage No. Ear Punch)	Sex	OCT (Clinical Findings)
1	6785 L1	F	Paracentral thinning
2	6785 L2	F	Small eye, central thinning
3	6785 R1	F	Normal
4	6785 No ear punch (0)	F	Normal
5	6785 R2	F	Thin cornea, iris attached, scarring
6	4569 R1	F	Paracentral thinning
7	4569 R1	M	Paracentral thinning
8	4569 0	M	Normal
9	4569 R2	M	Normal
10	4569 r1L1	M	Localized thinning at the periphery
11	6761 L1	M	Central thinning & scarring
12	6761 R1L1	M	Sever scarring and thinning
13	6761 L2	M	Localized thinning at the periphery
14	6761 R1	M	Paracentral l thinning
15	2573 0	M	Thin cornea
16	2573 R1	M	Localized central thinning
17	2573 L1	F	Localized thinning at the periphery
18	2573 R2	F	Central thinning
19	9019 0	M	Localized thinning at the periphery
20	9019 R1	M	Paracentral thinning
21	9019 R2	M	Paracentral thinning & scarring
22	9019 L1	M	Sever scarring and thinning
23	9019 R1L1	F	Paracentral thinning
24	9019 L2	F	Paracentral thinning

Two mice from the control group showed localized loss of epithelium, but the rest of the animals were normal when observed using OCT.

Investigative Ophthalmology & Visual Science

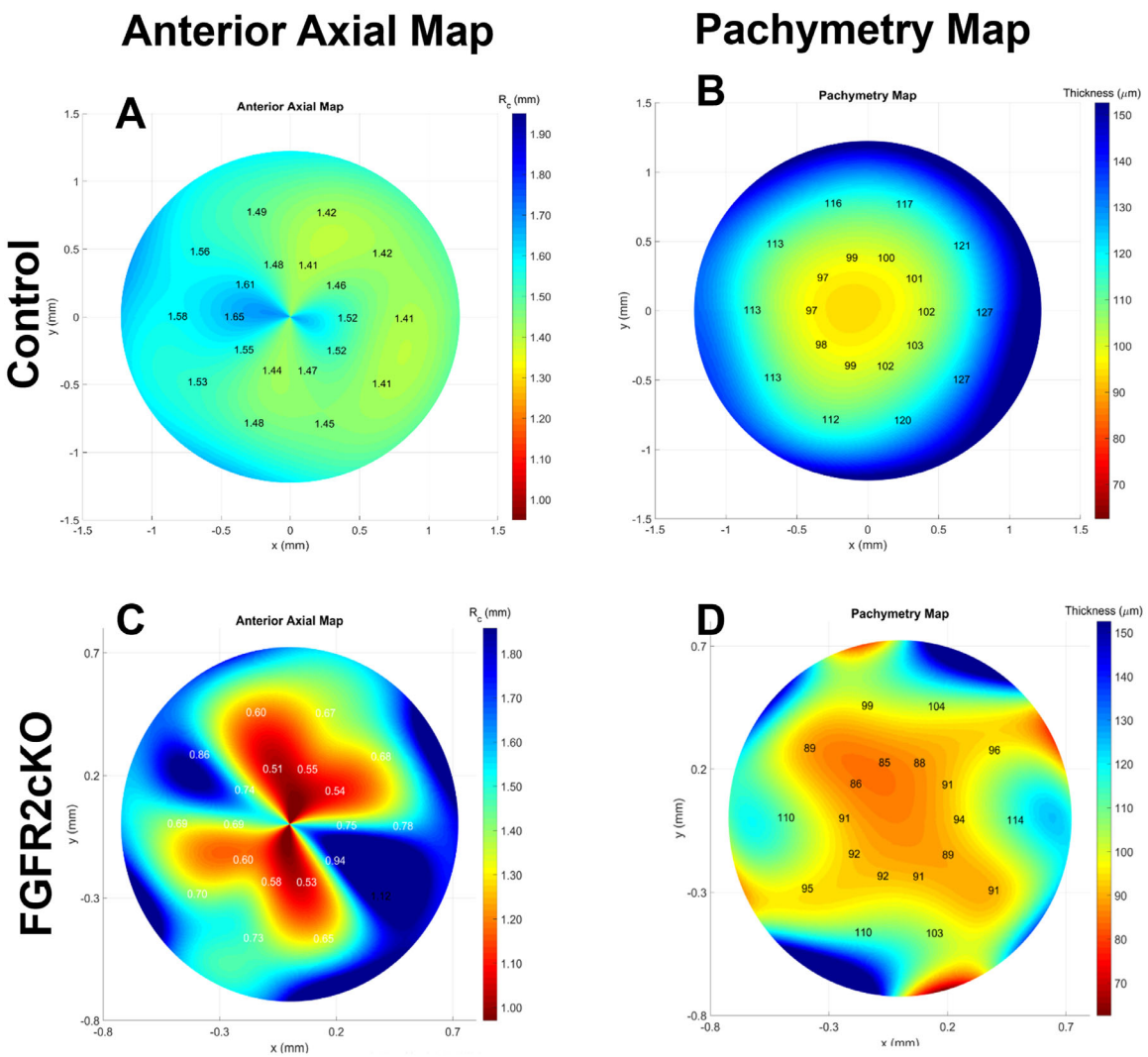

Figure 5. Representative corneal topography (axial maps) and pachymetry maps of control- and FGFR2cKO mice. **(A)** Representative corneal topography map of cornea of a control mouse. **(B)** Representative pachymetry map of cornea of a control mouse. **(C)** Representative corneal topography map of a FGFR2cKO mice showing an increased steepness (red color). **(D)** Representative pachymetry map of cornea of a FGFR2cKO mouse showing localized corneal thinning compared to control mice.

OCT analysis, next we analyzed relative collagen-1 expression in the cornea of one-month-old mice. Figures 6A-A′ and B-B′ show immunohistochemical localization of collagen-1 in the corneas of control and FGFR2cKO mice, respectively. Both control and FGFR2cKO mice corneas showed collagen-1 expression. When a small area (as depicted by an inset in Figs. 6A, 6B) were magnified in Figure 6A′ (control) and Figure 6B′ (FGFR2cKO), their immunostaining patterns in the control mice (Fig. 6A′) differed compared to that of FGFR2cKO mice (Fig. 6B′). Collagen-1 fibril staining seen in the control mice (Fig. 6A′) was absent in the FGFR2cKO mice (Fig. 6B′). This was further confirmed by Western blot analysis of collagen-1 expression in the corneal stroma of control- and FGFR2cKO mice, where a relative decrease in expression of collagen-1 in FGFR2cKO mouse relative to control mouse was observed (Fig. 6C). GAPDH was used as a loading control. The uncropped GAPDH is provided as Supplementary Figure S2. The above results of Western blot analysis were further confirmed on quantification of the band intensity by image J (shown by bar graph in Fig. 6D, n = 3 [$P < 0.05$]).

Increased Apoptosis at the Site of Corneal Thinning in FGFR2cKO Mice Relative to Control Mice

Because keratocyte loss has long been associated with KC development,[35] we examined the relative loss of keratocytes in the stroma of thee-month-old FGFR2cKO mice and control mice. Figure 7A shows a representative image of TUNEL staining in a control mouse-corneal section, which showed no TUNEL-staining of corneal cells. Figure 7B is an image of an OCT scan of FGFR2cKO mice, which showed central thinning in the cornea (identified by a yellow arrow). The mouse corneas were sectioned two weeks after OCT scans, and the corresponding regions that showed progressive thinning were used for analyzing cell death by TUNEL assay. Figure 7C shows the section of the region that exhibited corneal thinning in the OCT images, and the nuclei were counterstained with nuclear stain (4′,6-diamidino-2-phenylindole [DAPI]), and the orange arrow points to TUNEL-positive cells in the corneas of FGFR2cKO mice. Endothelial cells also showed TUNEL-positive staining in FGFR2cKO mice, but it

Investigative Ophthalmology & Visual Science

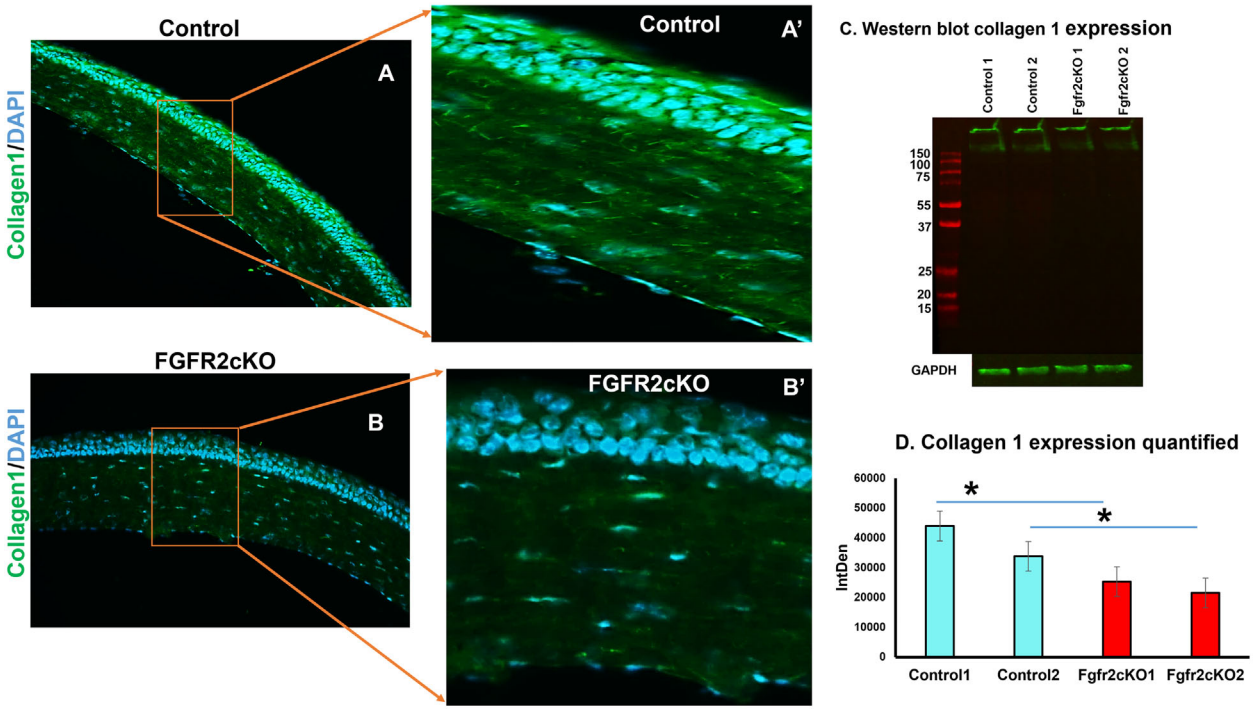

Figure 6. Representative collagen 1 expression in corneas of FGFR2cKO mice vs. control mice. (A) Collagen 1 expression and nuclear stain (DAPI) were co-localized in cornea of a control mouse. **(A′)** A small area (**inset**) is magnified to show the collagen 1 expression in cornea of a control mouse. **(B)** Collagen 1 expression and nuclear stain (DAPI) were co-localized in FGFR2cKO mice. **(B′)** a small area (**inset**) is magnified to show the collagen 1 expression in cornea of a FGFR2cKO mouse. Collagen 1 expression is decreased in FGFR2cKO mice relative to control mice. **(C)** Western blot analysis of Collagen 1 expression in control and FGFR2cKO mice. GAPDH was used as a loading control. **(D)** Quantification of collagen 1 expression in the Western blot using Image J (n = 3 [$P < 0.05$]).

was discontinuous. Because keratocytes showed a decrease in the corneal stroma of FGFR2cKO mice compared to the control mice, the keratocytes numbers were quantified by image J. As shown in Figure 7D, an increased number of apoptotic TUNEL-positive cells was also accompanied with fewer keratocytes in FGFR2cKO mice.

Acute Corneal Hydrops in FGFR2cKO Mice Relative to Control Mice

Acute corneal hydrops has been seen in patients who develop acute KC.[36–42] Therefore the corneas of three-month-old FGFR2cKO- and age-matched control mice were analyzed for corneal hydrops. Between 5% to 10% of the FGFR2cKO mice developed acute corneal hydrops, whereas the control mice showed no such development. Figure 8A shows the slit-lamp image of the cornea of a three-month-old FGFR2cKO mouse, which exhibited acute corneal hydrops, and Figure 8B further shows the region of hydrops in the cornea (identified by a red arrow). FGFR2cKO mice also showed acute scarring and edema. Because fibronectin expression is a marker of corneal fibrosis,[43] we analyzed fibronectin immunostaining in corneal section FGFR2cKO-mice that showed corneal hydrops. Figures 8C and 8D show fibronectin immunostaining in corneas of a control- and FGFR2cKO mice, respectively. An increased fibronectin immunostaining was observed in the corneal stromal region (shown by a green arrow) in FGFR2cKO mice (Fig. 8D) relative to control mice (Fig. 8C). Additionally, breaks in the Descemet's membrane with a large stromal cleft in FGFR2cKO mice with corneal hydrops were also observed (shown by a blue arrow in Fig. 8D). Figure 8D′ shows the remaining portion of the corneal section of Figure 8D, and the yellow arrow points to the endothelium, and the yellow star points to breaks in the endothelium in FGFR2cKO mouse cornea (Fig. 8D′). We also analyzed αSMA (alpha smooth muscle actin) expression in both control and FGFR2cKO mice (Figs. 8E–G). An increased expression of αSMA in the regions of scarring (white arrow, Fig. 8G), and breaks in the Descemet's membrane and the endothelium were seen in corneas of FGFR2cKO mice relative to control mice.

Transmission Electron Microscopic Analyses of the FGFR2cKO Mice and the Control Mice

We analyzed the distribution of collagen fibers at the apical corneal region using an transmission electron microscopy because earlier report has shown a large-scale directional changes in the collagen fibers during KC development.[44] Figure 9A shows an electron micrograph of control cornea whereas 9B is that of the FGFR2cKO mice cornea (yellow arrow shows collagen fibers in Figs. 9A, 9B). The cornea of FGFR2cKO mice showed characteristic features that are seen in human KC corneas (i.e., undulating lamellae, collagen fiber loss; blue arrow in Fig. 9C), and smaller fibrillar diameters compared to the control mice (Fig. 9D). The average collagen diameters in normal corneas were 34.4 ± 5.1 nm whereas in FGFR2cKO mice these were 16.9 ± 3.2 nm. Additionally, keratocytes seem to be crushed in the undulating lamellae in FGFR2cKO mice (red arrow in Fig. 9D) compared to normal keratocytes in the control mice (Fig. 9A).

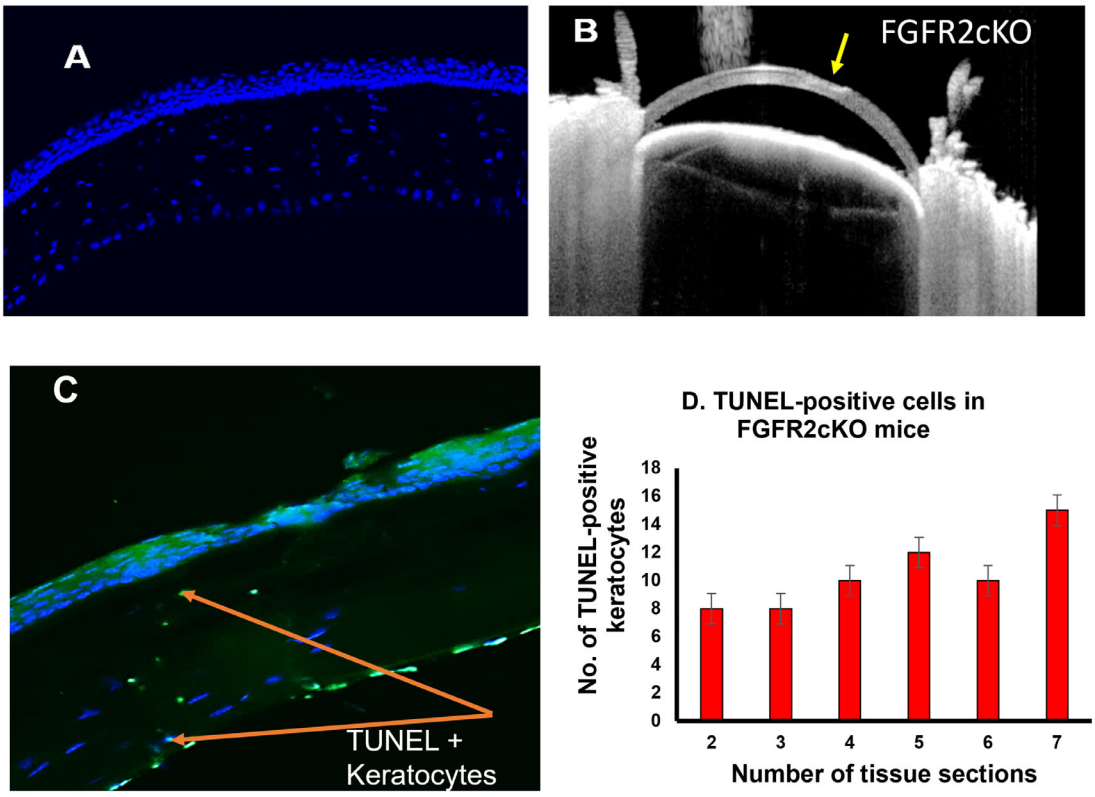

Figure 7. Detection of cellular apoptosis using TUNEL assay in the corneas of 3-month-old FGFR2cKO mice compared to control mice. **(A)** The stroma of control mice did not show any TUNEL-positive stained cells. **(B)** OCT image of FGFR2cKO mice that showed localized thinning (*yellow arrow*). (C) The same FGFR2cKO mice (in **B**) exhibited keratocytes' apoptosis in the stroma at the site of localized thinning. The apoptotic TUNEL-positive cells were also detected in the epithelium and endothelium, but these were discontinuously distributed in both layers of FGFR2cKO mice. **(D)** Apoptotic TUNEL-positive keratocytes number were quantified by their counting under a fluorescent microscope. Note that keratocytes numbers were decreased in the corneal stroma of FGFR2cKO compared to the control mice ($P < 0.05$).

Discussion

KC is a condition of unknown cause in which the cornea assumes a semi conical shape as a result of noninflammatory thinning of central or paracentral corneal stroma.[45] Recent literature suggests that an inflammatory component is also associated in KC.[46,47] Currently, there is no animal model available to determine the molecular mechanism for human KC development. We previously generated a human stem cell model that showed relative downregulation of FGFR2 in the stromal keratocytes of KC corneas compared to normal corneas.[3] Although keratocytes produce the corneal stromal components (collagen and proteoglycans, etc.) to maintain corneal transparency,[48] the role of FGFR2-signaling pathway in corneal stromal physiology and KC-development remains elusive. Earlier reports have shown that the germ-line Fgfr2b-knockout mice die shortly after birth due to multiple-organ abnormalities, such as agenesis of the lungs, limbs, anterior pituitary gland, thyroid gland and dysgenesis of the skin, glandular stomach, pancreas, and thymus.[49,50] The genetic alterations of FGFR2 at germline or somatic level give rise to congenital disorders and acquired diseases through dysregulation of FGFR2-signaling cascades.[51–53] Furthermore, FGFR2 seems to play important roles in eye tissues development. For example, FGFR2 signaling has been shown to be crucial for lens development,[22] and a FGFR2-conditional knockout mouse model, generated using a lens-Cre mice, showed abnormal corneal epithelium development but no major changes to the corneal stromal cells.[54] This difference in relative abnormalities in epithelium vs. stroma might be due to because the lens epithelial cells and corneal epithelial cells are derived from the surface ectodermal cells, whereas corneal stromal cells and corneal endothelial cells are derived from neural crest-derived mesenchymal cells. Because the function of FGFR2 in the corneal stromal development is presently unknown, we generated a novel knockout mouse model in which FGFR2 was conditionally deleted in corneal keratocytes using a keratocyte specific-keratocan Cre mice at postnatal day one. This Cre mouse was selected because keratocan expression is a phenotypic marker for keratocytes,[55] and therefore, its expression is limited to the corneal stroma.

Our homozygous mice for $Fgfr2^{flox}$ allele possessed loxP-sites flanking exons 8 to10. FGFR2 has two splice variants: FGFR2iiib and FGFR2iiic (Fig. 1B), which are generated due to an alternative splicing of exon 8 and 9. These splice variants differ in ligand binding (Fig. 1B), and, although FGFR2iiib is mainly expressed in the epithelium, FGFR2iiiC is expressed in the mesenchymal cells.[56,57] The $Fgfr2^{flox/flox}$ mice were bred to mice expressing Cre recombinase, resulting offspring that have sequence encoding the alternatively spliced Ig domain IIIb, as well the IIIc, and the TM domain deleted in the Cre-expressing tissues. Because our Cre-expressing animal was specific for mesenchymal cell–derived tissues (i.e., corneal stroma), we expected

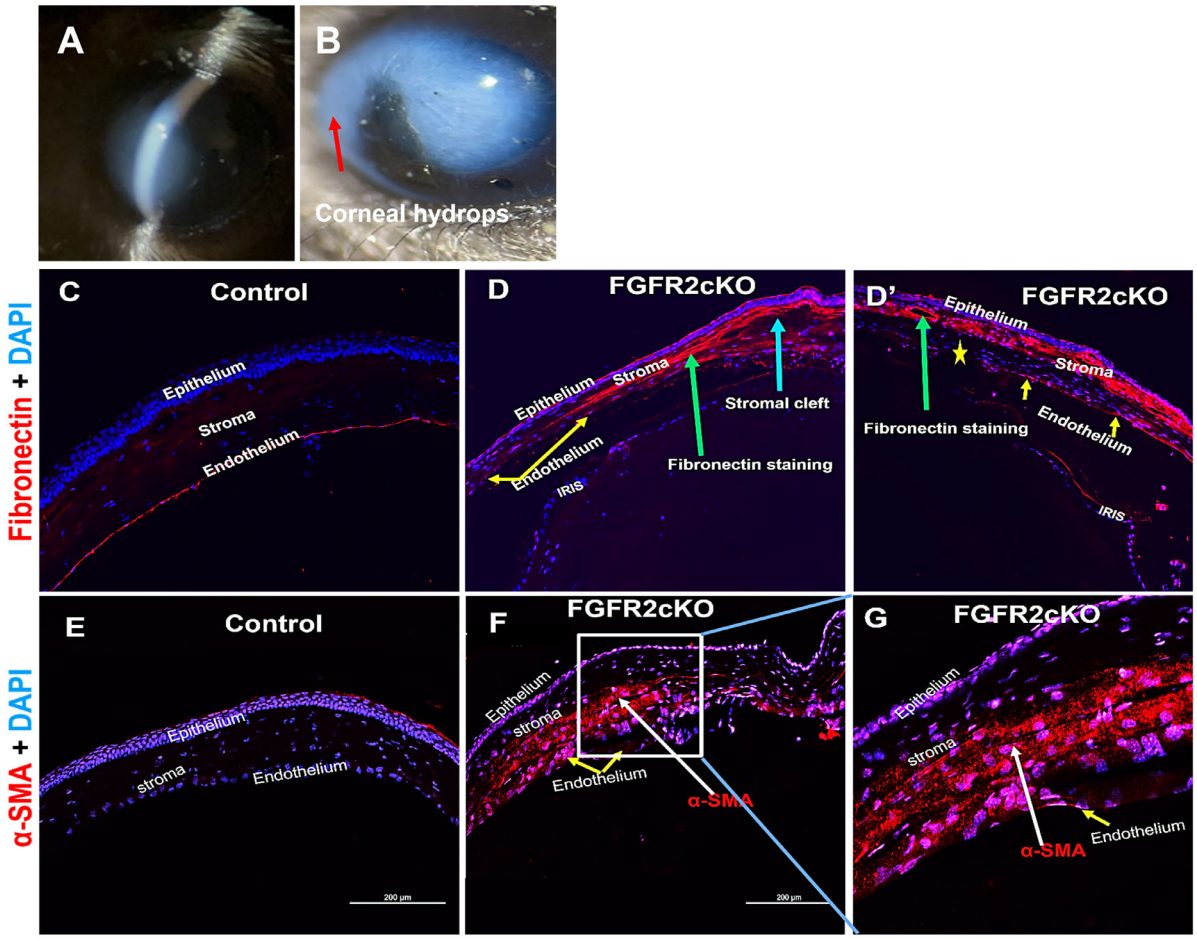

Figure 8. FGFR2cKO mice developed acute corneal hydrops, which were absent in control mice. **(A)** Slit lamp examination of FGFR2cKO mice that developed acute corneal hydrops. **(B)** Image of acute corneal hydrops (*red arrow*) in FGFR2cKO mice. These mice also showed corneal scarring. **(C)** Immunohistochemical colocalization of fibronectin expression with nuclear (DAPI) staining in control mice. **(D)** Immunohistochemical colocalization of fibronectin expression (*green arrow*) with nuclear (DAPI) staining at the region of corneal hydrops. An increased fibronectin expression at site of corneal hydrops **(D)** along with a large intra-stromal cleft (yellow arrow) was observed. **(D′)** The rest of the corneal section of **D**. The *yellow star* shows the region with the loss of endothelial cells. **(E)** Immunohistochemical colocalization of expression of alpha smooth muscle actin (αSMA) and nuclear Hoechst's staining in the cornea of a control mouse. **(F)** Immunohistochemical colocalization of expression of αSMA (*red stain*) with nuclear Hoechst's staining of the cornea of a FGFR2cKO mouse. **(G)** A small section (**inset**) of **F** that was magnified to show the staining in αSMA in the stroma.

that only the mesenchymal-expressing FGFR2 would be knocked down. Our result strongly concurs with this expectation, because the normal mouse corneas showed FGFR2-expression in all three corneal cell types—epithelium, stroma, and endothelium (Fig. 2A)—but in contrast, its expression was decreased only in the stromal keratocytes of FGFR2cKO mice. Previous reports have shown that the expression of keratocan gene in mice begins as early as at E13.5 in periocular mesenchymal cells migrating toward the cornea and sclera, but its expression gradually becomes restricted to corneal keratocytes at E18.5 in the adult mice.[58] Periocular mesenchymal cells give rise to both endothelial cells and keratocytes. The absence of FGFR2 expression in the endothelium of the knockout mice could be due to feeding of doxycycline early on during mouse development. Furthermore, the newly generated novel FGFR2cKO mice were healthy and fertile, unlike previously generated germ-cell line FGFR2-mutated mice.

The one major finding of this study was that the FGFR2cKO mice exhibited several human KC phenotypes relative to control mice during their corneal examinations by a variety of techniques. The KC-specific phenotypic changes in corneas of FGFR2cKO mice relative to control mice included: (A) localized central corneal thinning; (B) altered corneal curvature with an increased corneal steepness and altered corneal thickness during axial maps and pachymetric maps analyses, respectively; (C) reduced collagen-1 fibril staining and its reduced expression in stromal region; (D) undulating lamellae, collagen fiber loss with smaller fibrillar diameters; (E) acute corneal hydrops; and (F) apoptotic loss of keratocytes.

OCT has become an important noninvasive, high-resolution imaging modality in the assessment of the cornea and eye anterior segment and is therefore a critical tool in the diagnosis of KC and other corneal ectatic diseases.[59,60] The novel FGFR2cKO mice exhibited peripheral corneal thinning at P31 days during ANTERION OCT examination (Figs. 3C, 3D). To our surprise, the same mice, when imaged later at the P90 stage, developed a central corneal thinning as shown in Figures 3G and 3H. The development of

Investigative Ophthalmology & Visual Science

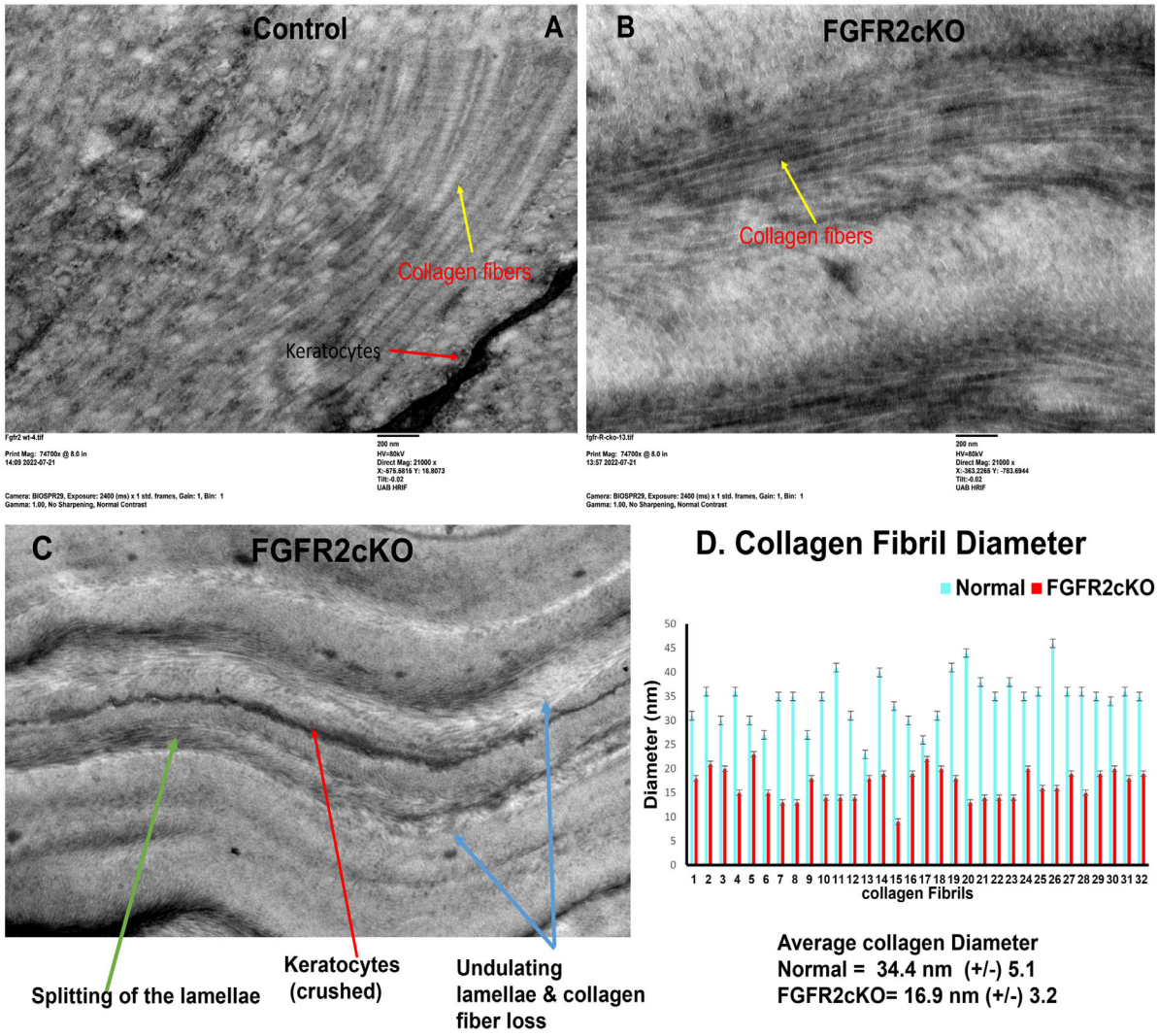

Figure 9. Representative transmission electron micrographs of corneas of FGFR2cKO mice versus control mice. **(A)** Electron micrograph of the apical region cornea (200 nm) of a control mouse. The *yellow arrow* points to the collagen fibrils in the control cornea. **(B)** Electron micrograph of the apical region of cornea of a FGFR2cKO mouse (200 nm). The *yellow arrow* points to the collagen fibrils in the FGFR2cKO cornea. Lamellar splitting into multiple bundles of collagen fibrils and loss of lamellae was seen in FGFR2cKO cornea relative control cornea. **(C)** Shows undulating lamellae in the FGFR2cKO mice compared to control. **(D)** Collagen fibril diameters measured at the apical region of corneal thinning from the electron micrographs using image J for both control nice (*blue*) and FGFR2cKO mice (*red*) and is plotted as a bar graph (n = 3 [$P < 0.05$]).

central corneal thinning at three months of age in FGFR2cKO mice does correlate to the general appearance of KC in human teenagers, based on comparison of the life spans of mice versus humans.[61] Presently there are no data in the literature available that shows whether very young children, destined to future development of KC, undergo a prior phase of peripheral corneal thinning before clinical manifestation of central thinning at the teenage years. However, a prior report has also shown that KC affects a wider area of the cornea, but the corneal ectasia shows the greatest changes in thickness, and this attenuation declines to the periphery.[62] Therefore the FGFR2cKO mouse model would provide the valuable insight into the KC-specific progression of corneal thinning from the peripheral to central region.

Corneal topography is a valuable technique to analyze the characteristics of the cornea such as shape, curvature, power, and thickness. The primary technologies used in modern corneal topography are Placido disc, Scheimpflug and scanning-slit topography. Corneal topographers provide different maps to represent the measurements that characterize the surface of a KC cornea. Because of an absence of a commercially available mouse corneal topography analysis instrument, we used a Spectral Domain-OCT-based anterior curvature and thickness mapping analysis method as previously developed by Liu et al.[33] Because the ANTERION OCT files could not be used for corneal topography mapping, we switched to the Spectral Domain-OCT method. Corneal topographical analysis program has been successfully used by other groups to determine corneal topography and pachymetry mapping in mouse models to study its relationship with KC.[63] The FGFR2cKO mice showed abnormal corneal curvature and localized thinning compared to control mice (Figs. 5C, 5D). We were able to demonstrate

Investigative Ophthalmology & Visual Science

a color-coded pattern like that seen in corneal topographic maps from a human KC cornea.

Collagen in the stroma is predominantly type I, with smaller amounts of types V, VI, XII, XIII, XIV, and XXIV.[64] KC corneas show gross organization loss of the stromal lamellae compared to normal corneas.[44] It has been shown that in the corneal endothelium, the FGF2-mediated signaling induces the secretion of type-1 collagen, the major component of the retro-corneal fibrous membrane.[65,66] Our analysis also showed that collagen-1 expression decreased in FGFR2cKO mice compared to control mice (Fig. 6), and this could be due to the loss of FGFR2-mediated signaling in the corneal keratocytes with yet unknown mechanism. We further showed that the gross organization of stromal lamellar collagen 1 was relatively reduced in the FGFR2cKO mice (Fig. 6B′) compared to the control mice (Fig. 6A′).

Keratocytes' apoptosis has been associated with KC,[35,67] but causative factors leading to the apoptotic loss of keratocytes remain elusive. We previously hypothesized that KC-keratocytes might undergo apoptosis because of the downregulation of FGFR2-mediated signaling.[3] This was also supported by previous reports that showed that inhibition of FGFR2-mediated signaling induced apoptosis in several cancer cells.[68–70] The FGFR2cKO mice also showed increased apoptotic loss of keratocytes at the region exhibiting localized corneal thinning compared to control mice (Fig. 7). Usually keratocyte apoptosis is followed by a wound healing response,[71] but the FGFR2cKO mice also showed an impaired wound healing response as seen by fewer keratocytes compared to control. This coincides with the earlier reports that showed KC keratocytes have poor growth and survival in serum-free media relative keratocytes from normal human corneas.[3,72]

Corneal hydrops is a complication associated with advanced KC and is seen in approximately 3% of eyes with KC.[41] Some of the FGFR2cKO mice also developed acute corneal hydrops (Fig. 8), which was also accompanied by a relative increased fibronectin expression in these mice along with breaks in the Descemet's membrane (Fig. 8D) relative to control mice (Fig. 8C). Reports show significant scar and corneal edema association with corneal hydrops in patients with acute KC.[36–42] Therefore FGFR2cKO mice with acute corneal hydrops and phenotypic characteristics were similar as seen in patients with acute KC with corneal hydrops.

Studies have shown that the mechanical strength and the corneal transparency are governed by the ability of collagen fibrils to assemble into organized lamellae and is under the influence of proteoglycans controlling the fibril diameter and biosynthesis.[73,74] Electron microscopic images have shown that KC corneas have an undulating lamella.[75,76] Similarly, the corneas of FGFR2cKO mice also showed an irregular or wavy orientation of the lamellae compared to a control mouse (Figs. 9A, 9B). Earlier electron microscopic micrographs have also shown that the irregularities of corneal collagen lamellae were not caused by an artifact.[76] Changes in the lamellar arrangement have been seen to play a role in the thinning of the cornea, and our TEM analysis of FGFR2cKO mice strongly suggest altered lamellar architecture and altered collagen diameters that could play a role in the corneal thinning process (Fig. 9).

In summary, our novel FGFR2cKO mouse model showed several phenotypic characteristics that are similarly seen during human KC development (localized thinning, changes in the corneal topography, altered collagen lamellae organization, keratocytes' apoptosis, corneal hydrops, and potential corneal fibrosis). The evidence presented herein strongly suggest that the FGFR2cKO mouse model could be used as a model to study FGFR2-signaling pathway to understand the molecular mechanism of FGFR2-induced KC development and to provide an opportunity for therapeutic interventions during KC development.

Acknowledgments

The authors thank Rafael Grytz, PhD (Department of Ophthalmology and Visual Sciences, UAB), for helping us in the ANTERION OCT and Michael Boulton PhD (Department of Ophthalmology and Visual Sciences, UAB), for allowing us to use the SD-OCT instrument. Anthony N. Kuo MD (Department of Ophthalmology, Duke) for providing us the corneal topography analysis program.

Supported by P30-EY03039.

Disclosure: **R. Joseph**, None; **A. Boateng**, None; **O.P. Srivastava**, None; **R.R. Pfister**, None

References

1. US NEI. Facts about the cornea and corneal disease keratoconus.
2. Kennedy RH, Bourne WM, Dyer JA. A 48-year old clinical epidemiological study of keratoconus. *Am J Ophthalmol*. 1986;10:267–273.
3. Joseph R, Srivastava OP, Pfister RR. Modeling keratoconus using induced pluripotent stem cellsmodeling keratoconus using iPSC. *Invest Ophthalmol Vis Sci*. 2016;57:3685–3697.
4. Roessler R, Smallwood Sebastien A, Veenvliet Jesse V, et al. Detailed analysis of the genetic and epigenetic signatures of iPSC-derived mesodiencephalic dopaminergic neurons. *Stem Cell Reports*. 2014;2:520–533.
5. Ortega S, Ittmann M, Tsang SH, Ehrlich M, Basilico C. Neuronal defects and delayed wound healing in mice lacking fibroblast growth factor 2. *Proc Natl Acad Sci USA*. 1998;95:5672.
6. Goetz R, Mohammadi M. Exploring mechanisms of FGF signalling through the lens of structural biology. *Nat Rev Mol Cell Biol*. 2013;14:166–180.
7. Eswarakumar VP, Lax I, Schlessinger J. Cellular signaling by fibroblast growth factor receptors. *Cytokine Growth Factor Rev*. 2005;16:139–149.
8. Turner N, Grose R. Fibroblast growth factor signalling: from development to cancer. *Nat Rev Cancer*. 2010;10:116–129.
9. Beenken A, Mohammadi M. The FGF family: biology, pathophysiology and therapy. *Nat Rev Drug Discov*. 2009;8:235–253.
10. Peters KG, Marie J, Wilson E, et al. Point mutation of an FGF receptor abolishes phosphatidylinositol turnover and Ca2+ flux but not mitogenesis. *Nature*. 1992;358:678–681.
11. Feldman B, Poueymirou W, Papaioannou VE, DeChiara TM, Goldfarb M. Requirement of FGF-4 for postimplantation mouse development. *Science*. 1995;267:246–249.
12. Arman E, Haffner-Krausz R, Chen Y, Heath JK, Lonai P. Targeted disruption of fibroblast growth factor (FGF) receptor 2 suggests a role for FGF signaling in pregastrulation mammalian development. *Proc Natl Acad Sci USA*. 1998;95:5082–5087.
13. Cheng AM, Saxton TM, Sakai R, et al. Mammalian Grb2 regulates multiple steps in embryonic development and malignant transformation. *Cell*. 1998;95:793–803.
14. Hadari YR, Gotoh N, Kouhara H, Lax I, Schlessinger J. Critical role for the docking-protein FRS2α in FGF receptor-

mediated signal transduction pathways. *Proc Natl Acad Sci USA*. 2001;98:8578–8583.
15. Saba-El-Leil MK, Vella FD, Vernay B, et al. An essential function of the mitogen-activated protein kinase Erk2 in mouse trophoblast development. *EMBO Rep*. 2003;4:964–968.
16. Hatano N, Mori Y, Oh-Hora M, et al. Essential role for ERK2 mitogen-activated protein kinase in placental development. *Genes to Cells*. 2003;8:847–856.
17. Helsten TL, Elkin SK, Carter J, Kurzrock R. The FGFR landscape in cancer: an analysis of 4,869 cases. *J Clin Oncol*. 2014;32:11059–11059.
18. Liu CY, Francis JH, Abramson DH. Ocular side effects of systemically administered chemotherapy. *UPToDate* 2019.
19. Campochiaro PA, Chang M, Ohsato M, et al. Retinal degeneration in transgenic mice with photoreceptor-specific expression of a dominant-negative fibroblast growth factor receptor. *J Neurosci*. 1996;16:1679.
20. Reneker LW, Wang L, Irlmeier RT, Huang AJW. Fibroblast growth factor receptor 2 (FGFR2) is required for meibomian gland homeostasis in the adult mousethe role of FGF receptor 2 in meibomian gland homeostasis. *Invest Ophthalmol Vis Sci*. 2017;58:2638–2646.
21. Smith KM, Williamson TL, Schwartz ML, Vaccarino FM. Impaired motor coordination and disrupted cerebellar architecture in Fgfr1 and Fgfr2 double knockout mice. *Brain Res*. 2012;1460:12–24.
22. Garcia CM, Yu K, Zhao H, et al. Signaling through FGF receptor-2 is required for lens cell survival and for withdrawal from the cell cycle during lens fiber cell differentiation. *Dev Dyn*. 2005;233:516–527.
23. Ever L, Zhao R, Eswarakumar VP, Gaiano N. Fibroblast growth factor receptor 2 plays an essential role in telencephalic progenitors. *Dev Neurosci*. 2008;30:306–318.
24. Zhang Y, Kao WW, Hayashi Y, et al. Generation and characterization of a novel mouse line, keratocan-rtTA (KeraRT), for corneal stroma and tendon research. *Invest Ophthalmol Vis Sci*. 2017;58:4800–4808.
25. Yu K, Xu J, Liu Z, et al. Conditional inactivation of FGF receptor 2 reveals an essential role for FGF signaling in the regulation of osteoblast function and bone growth. *Development*. 2003;130:3063–3074.
26. Joseph R, Srivastava OP, Pfister RR. Downregulation of β-Actin gene and human antigen R in human keratoconus. *Invest Ophthalmol Vis Sci*. 2012;53:4032–4041.
27. Hanlon SD, Patel NB, Burns AR. Assessment of postnatal corneal development in the C57BL/6 mouse using spectral domain optical coherence tomography and microwave-assisted histology. *Exp Eye Res*. 2011;93:363–370.
28. Han SB, Liu Y-C, Noriega KM, Mehta JS. Applications of anterior segment optical coherence tomography in cornea and ocular surface diseases. *J Ophthalmol*. 2016;2016:4971572.
29. Wang J, Saul A, Cui X, Roon P, Smith SB. Absence of sigma 1 receptor accelerates photoreceptor cell death in a murine model of retinitis pigmentosa. *Invest Ophthalmol Vis Sci*. 2017;58:4545–4558.
30. Deerinck TJ, Bushong EA, Lev-Ram V, Shu X, Tsien RY, Ellisman MH. Enhancing Serial Block-Face Scanning Electron Microscopy to Enable High Resolution 3-D Nanohistology of Cells and Tissues. *Microsc Microanal*. 2010;16:1138–1139.
31. Graham RC, Karnovsky MJ. THF early stages of absorption of injected horseradish peroxidase in the proximal tubules of mouse kidney: ultrastructural cytochemistry by a new technique. *J Histochem Cytochem*. 1966;14:291–302.
32. Fortier SM, Penke LR, King D, Pham TX, Ligresti G, Peters-Golden M. Myofibroblast dedifferentiation proceeds via distinct transcriptomic and phenotypic transitions. *JCI Insight*. 2021;6(6):e144799.
33. Liu AS, Brown DM, Conn RE, McNabb RP, Pardue MT, Kuo AN. Topography and pachymetry maps for mouse corneas using optical coherence tomography. *Exp Eye Res*. 2020;190:107868.
34. Shetty R, Sathyanarayanamoorthy A, Ramachandra RA, et al. Attenuation of lysyl oxidase and collagen gene expression in keratoconus patient corneal epithelium corresponds to disease severity. *Mol Vis*. 2015;21:12.
35. Kim W-J, Rabinowitz YS, Meisler DM, Wilson SE. Keratocyte apoptosis associated with keratoconus. *Exp Eye Res*. 1999;69:475–481.
36. Tuft SJ, Gregory WM, Buckley RJ. Acute corneal hydrops in keratoconus. *Ophthalmology*. 1994;101:1738–1744.
37. Maharana PK, Sharma N, Vajpayee RB. Acute corneal hydrops in keratoconus. *Indian J Ophthalmol*. 2013;61:461–464.
38. Fan Gaskin JC, Patel DV, McGhee CNJ. Acute corneal hydrops in keratoconus—new perspectives. *Am J Ophthalmol*. 2014;157:921–928.e921.
39. Barsam A, Petrushkin H, Brennan N, et al. Acute corneal hydrops in keratoconus: a national prospective study of incidence and management. *Eye (London, England)*. 2015;29:469–474.
40. Ng H, Mathan J, Patel DV. Acute corneal hydrops in a young man. *JAMA Ophthalmol*. 2020;138:e190960–e190960.
41. Aldave AJ, Mabon M, Hollander DA, McLeod SD, Spencer WH, Abbott RL. Spontaneous corneal hydrops and perforation in keratoconus and pellucid marginal degeneration. *Cornea*. 2003;22:169–174.
42. Makino S. Acute corneal hydrops in a patient with intellectual disability. *BMJ Case Rep*. 2014;2014:bcr2014205782.
43. Karamichos D, Guo XQ, Hutcheon AEK, Zieske JD. Human corneal fibrosis: an in vitro model. *Invest Ophthalmol Vis Sci*. 2010;51:1382–1388.
44. Meek KM, Tuft SJ, Huang Y, et al. Changes in collagen orientation and distribution in keratoconus corneas. *Invest Ophthalmol Vis Sci*. 2005;46:1948–1956.
45. Krachmer JH, Feder RS, Belin MW. Keratoconus and related noninflammatory corneal thinning disorders. *Surv Ophthalmol*. 1984;28:293–322.
46. Galvis V, Sherwin T, Tello A, Merayo J, Barrera R, Acera A. Keratoconus: an inflammatory disorder? *Eye (Lond)*. 2015;29:843–859.
47. Berger T, Szentmáry N, Chai N, et al. In vitro expression analysis of cytokines and ROS-related genes in human corneal fibroblasts and keratocytes of healthy and keratoconus corneas. *Ocul Immunol Inflamm*. 2023;1–10.
48. Hassell JR, Birk DE. The molecular basis of corneal transparency. *Exp Eye Res*. 2010;91:326–335.
49. De Moerlooze L, Spencer-Dene B, Revest J, Hajihosseini M, Rosewell I, Dickson C. An important role for the IIIb isoform of fibroblast growth factor receptor 2 (FGFR2) in mesenchymal-epithelial signalling during mouse organogenesis. *Development*. 2000;127:483–492.
50. Revest J-M, Spencer-Dene B, Kerr K, De Moerlooze L, Rosewell I, Dickson C. Fibroblast growth factor receptor 2-IIIb acts upstream of Shh and Fgf4 and is required for limb bud maintenance but not for the induction of Fgf8, Fgf10, Msx1, or Bmp4. *Dev Biol*. 2001;231:47–62.
51. Grose R, Dickson C. Fibroblast growth factor signaling in tumorigenesis. *Cytokine Growth Factor Rev*. 2005;16:179–186.
52. Wilkie AOM. Bad bones, absent smell, selfish testes: the pleiotropic consequences of human FGF receptor mutations. *Cytokine Growth Factor Rev*. 2005;16:187–203.
53. Katoh M. Cancer genomics and genetics of FGFR2 (review). *Int J Oncol*. 2008;33:233–237.

Investigative Ophthalmology & Visual Science

54. Zhang J, Upadhya D, Lu L, Reneker LW. Fibroblast growth factor receptor 2 (FGFR2) is required for corneal epithelial cell proliferation and differentiation during embryonic development. *PLoS ONE*. 2015;10:e0117089.
55. Carlson EC, Liu C-Y, Chikama T-i, et al. Keratocan, a cornea-specific keratan sulfate proteoglycan, is regulatedby lumican*. *J Biol Chem*. 2005;280:25541–25547.
56. Orr-Urtreger A, Bedford MT, Burakova T, et al. Developmental localization of the splicing alternatives of fibroblast growth factor receptor-2 (FGFR2). *Dev Biol*. 1993;158:475–486.
57. Gong SG. Isoforms of receptors of fibroblast growth factors. *J Cell Physiol*. 2014;229:1887–1895.
58. Liu C-Y, Shiraishi A, Kao CWC, et al. The cloning of mouse keratocan cDNA and genomic DNA and the characterization of its expression during eye development*. *J Biol Chem*. 1998;273:22584–22588.
59. Nakagawa T, Maeda N, Higashiura R, Hori Y, Inoue T, Nishida K. Corneal topographic analysis in patients with keratoconus using 3-dimensional anterior segment optical coherence tomography. *J Cataract Refract Surg*. 2011;37:1871–1878.
60. Huang D, Swanson EA, Lin CP, et al. Optical coherence tomography. *Science*. 1991;254:1178–1181.
61. Dutta S, Sengupta P. Men and mice: relating their ages. *Life Sci*. 2016;152:244–248.
62. Brautaset RL, Nilsson M, Miller WL, Leach NE, Tukler JH, Bergmanson JP. Central and peripheral corneal thinning in keratoconus. *Cornea*. 2013;32:257–261.
63. Khaled ML, Bykhovskaya Y, Gu C, et al. PPIP5K2 and PCSK1 are candidate genetic contributors to familial keratoconus. *Sci Rep*. 2019;9:19406.
64. Ihanamäki T, Pelliniemi LJ, Vuorio E. Collagens and collagen-related matrix components in the human and mouse eye. *Prog Retin Eye Res*. 2004;23:403–434.
65. Leung EW, Rife L, Smith RE, Kay EP. Extracellular matrix components in retrocorneal fibrous membrane in comparison to corneal endothelium and Descemet's membrane. *Mol Vis*. 2000;6:15–23.
66. Kay EP, Gu X, Smith RE. Corneal endothelial modulation: bFGF as direct mediator and corneal endothelium modulation factor as inducer. *Invest Ophthalmol Vis Sci*. 1994;35:2427–2435.
67. Kaldawy RM, Wagner J, Ching S, Seigel GM. Evidence of apoptotic cell death in keratoconus. *Cornea*. 2002;21:206–209.
68. Byron SA, Gartside MG, Wellens CL, et al. Inhibition of activated fibroblast growth factor receptor 2 in endometrial cancer cells induces cell death despite PTEN abrogation. *Cancer Res*. 2008;68:6902–6907.
69. Kunii K, Davis L, Gorenstein J, et al. FGFR2-amplified gastric cancer cell lines require FGFR2 and Erbb3 signaling for growth and survival. *Cancer Res*. 2008;68:2340–2348.
70. Ando K, Ohira M, Takada I, et al. FGFR2 loss sensitizes MYCN-amplified neuroblastoma CHP134 cells to CHK1 inhibitor-induced apoptosis. *Cancer Sci*. 2022;113:587–596.
71. Wilson SE, Kim WJ. Keratocyte apoptosis: implications on corneal wound healing, tissue organization, and disease. *Invest Ophthalmol Vis Sci*. 1998;39:220–226.
72. Foster J, Wu W-H, Scott S-G, et al. Transforming growth factor β and insulin signal changes in stromal fibroblasts of individual keratoconus patients. *PLoS ONE*. 2014;9:e106556.
73. Meek KM, Knupp C. Corneal structure and transparency. *Prog Retin Eye Res*. 2015;49:1–16.
74. Rada JA, Cornuet PK, Hassell JR. Regulation of corneal collagen fibrillogenesis in vitro by corneal proteoglycan (lumican and decorin) core proteins. *Exp Eye Res*. 1993;56:635–648.
75. Alkanaan A, Barsotti R, Kirat O, Khan A, Almubrad T, Akhtar S. Collagen fibrils and proteoglycans of peripheral and central stroma of the keratoconus cornea - Ultrastructure and 3D transmission electron tomography. *Sci Rep*. 2019;9:19963.
76. Polack FM. Contributions of electron microscopy to the study of corneal pathology. *Surv Ophthalmol*. 1976;20:375–414.

Investigative Ophthalmology & Visual Science